LBL-26570
Preprint

Lawrence Berkeley Laboratory
UNIVERSITY OF CALIFORNIA

Submitted to Physical Review C

Production of Helium (Z=2) Projectile Fragments in ^{16}O-Emulsion Interactions from E/A = 2 to 200 GeV

EMU-01 Collaboration

February 1989

Prepared for the U.S. Department of Energy under Contract Number DE-AC03-76SF00098.

LBL-26570

Production of Helium (Z=2) Projectile Fragments in ^{16}O-Emulsion Interactions from E/A = 2 to 200 GeV

EMU-01 Collaboration

Nuclear Science Division
Lawrence Berkeley Laboratory
1 Cyclotron Road
Berkeley, California 94720

February 1989

This work was supported by the Director, Office of Energy Research, Office of High Energy and Nuclear Physics, Division of Nuclear Physics of the U.S. Department of Energy under Contract DE-AC03-76SF00098.

Production of Helium (Z=2) Projectile Fragments in ^{16}O-Emulsion Interactions from E/A = 2 to 200 GeV

EMU-01 Collaboration

M.I. Adamovich,[10] M.M. Aggarwal,[3] R Arora,[3] Y.A.Alexandrov,[10]
S.A. Asimov,[14] E. Basova,[13] K.B. Bhalla,[5] A. Bhasin,[6]
V.S. Bhatia,[3] R.A. Bondarenkov,[13] T.H. Burnett,[12] X. Cai,[15]
L.P. Chernova,[14] M.M. Chernyavsky,[10] B. Dressel,[9]
E.M. Friedlander,[2] S.I. Gadzhieva,[14] E.R. Ganssauge,[9]
S. Garpman,[7] S.G. Gerassimov,[10] A. Gill,[5] J. Grote,[12]
K.G. Gulamov,[14] U.G. Gulyamov,[13] S. Hackel,[9] H.H. Heckman,[2]
B. Jakobsson,[7] B. Judek,[11] S. Kachroo,[6] F.G. Kadyrov,[14]
H. Kallies,[9] L. Karlsson,[7] G.L. Kaul,[6] M. Kaur,[3]
S.P. Kharlamov,[10] V. Kumar,[5] P. Lal,[5] V.G. Larionova,[10]
P.J. Lindstrom,[2] L.S. Liu,[15] S. Lokanathan,[5] J. Lord,[12]
N.S. Lukicheva,[14] L.K. Mangotra,[6] N.V. Maslennikova,[10]
I.S. Mittra,[3] E. Monnand,[1] S. Mookerjee,[5] C. Mueller,[9]
S.H. Nasyrov,[13] W.S. Navotny,[14] G.I. Orlova,[10] I. Otterlund,[7]
H.S. Palsania,[5] N.G. Peresadko,[10] S. Persson,[7] N.V. Petrov,[13]
W.Y. Qian,[15] R. Raniwala,[5] S. Raniwala,[5] N.K. Rao,[6] J.T. Rhee,[9]
N. Saidkhanov,[13] N.G. Salmanova,[10] W. Schulz,[9] F. Schussler,[1]
V.S. Shukla,[5] D. Skelding,[12] K. Soderstrom,[7] E. Stenlund,[7]
R.S. Storey,[11] J.F. Sun,[8] L.N. Svechnikova,[14] M.I. Tretyakova,[10]
T.P. Trofimova,[13] H.Q. Wang,[15] Z.O. Weng,[8] R.J. Wilkes,[12]
G.F. Xu,[1] D. H. Zhang,[8] P.Y. Zheng,[1] D.C. Zhou,[15] J.C. Zhou[15]

1) Beijing, Academica Sinica, Peoples Republic of China
2) Berkeley, Lawrence Berkeley Laboratory, USA
3) Chandigarh, Panjab University, India
4) Grenoble, C.E.N., France
5) Jaipur, University of Rajasthan, India
6) Jammu, University of Jammu, India
7) Lund, University of Lund, Sweden
8) Linfen, Shanxi Normal University, Peoples Republic of China
9) Marburg, Philipps University, West Germany
10) Moscow, Lebedev Physical Institute, USSR
11) Ottawa, National Research Council, Canada
12) Seattle, University of Washington, USA
13) Tashkent, Inst. Nucl. Phys., USSR
14) Taskent, Physical-Technical Inst., USSR
15) Wuhan, Hua-Zhong Normal University, Peoples Republic of China

ABSTRACT:

The fragmentation of relativistic ^{16}O projectiles in nuclear emulsion into projectile fragments (PFs) of $Z \geq 2$ has been investigated. Production rates, charge and multiplicity distribution of such PFs and their dependence on target-fragment multiplicities have been obtained. The width of the momentum distribution of He (Z=2) projectile fragment as well as the average number of target fragments is found to decrease with increasing He multiplicity. These dependences are, within errors of measurement, the same for E/A = 2.1, 14.6, 60 and 200 GeV, and to that extent satisfy the condition of limiting fragmentation.

INTRODUCTION:

The acceleration of ^{16}O ions to E/A = 60 and 200 GeV at CERN and 14.6 GeV at BNL heralds a significant advance in the field of relativistic heavy ion physics. In conjunction with the studies of particle production in interactions of ^{16}O with emulsion nuclei at 200A GeV by the EMU-01 collaboration for purposes of understanding hadronization in the nuclear environment [1], we have also examined interactions that exhibit the fragmentation of the incident ^{16}O nucleus. In such interactions, projectile fragments are essentially emitted inside a narrow forward angular cone centered around the direction of the incident ion at near beam velocity. The momentum, hence, approximately, the angular distributions are characteristically Gaussian-shaped. Their widths are, to a first approximation, governed by the Fermi motion of the nucleons within the fragmenting nucleus[2,3]. In this work we report on measurements on projectile and target fragmentation in emulsion chambers and stacks, with specific emphasis on the angular disribution of He (Z=2) projectile fragments (PFs) from peripheral ^{16}O-Em interactions at energies of 2, 15, 60 and 200 GeV/nucleon.

DETECTORS AND MEASURING DEVICES:

In late 1986 fifty emulsion chambers, 10 X 10 X 10 cm^3 in volume, and six high sensitivity (HS) stacks, up to 20 cm in length were exposed to the CERN SPS ^{16}O beam at energies E/A = 60 and 200 GeV. (For details see Refs. 1 and 4 and references therein.) In addition individual stacks of lower sensitive (LS) emulsion (yielding typically 6-8 grains/100μm for a minimum ionizing particles) were exposed to ^{16}O beams at E/A = 14.6, 60 and 200 GeV, respectively.

The measuring systems used in this work incorporate microscopes with digital readout of the xyz stage coordinates in 1 μm units (typically). With such systems, emission angles of projectile fragments are measured to accuracies $\sigma(\theta) \sim 3 \times 10^{-5}$ rad, or when expressed in terms of psuedorapidity, $\eta = -\ln(\tan\theta/2)$, $\sigma(\eta) \sim 0.1-0.2$ at $\eta=9$, the psuedorapidity characteristic of He PFs of ^{16}O at 200A GeV. Representative coordinates of all tracks (including those of the vertex) were measured relative to adjacent, non-interacting beam tracks, and subjected to least squares, 3-dimensional reconstruction programs that yield projected and space angles from which particle-multiplicity and pseudorapidity distributions were derived on an event-by-event basis.

SCANNING PRODEDURES:

In the emulsion stacks conventional "along-the-track" scanning was used to locate ^{16}O-Em interactions, The data sample thereby obtained is virtually unbiased. The charges of the emitted particles were determined by gap-length distributions and/or δ-ray densities (HS emulsions) and by photometric track width measurements and gap density distributions (LS emulsions). Data recorded for each event pertinent to this work include the multiplicities and emission angles of shower (Z=1) particles (HS emulsions only) and PFs with $Z \geq 2$. In addition, the number of heavily ionizing fragments having grain densities $g \geq 1.4\, g_{min}$ ($E_p \leq$ 400 MeV) associated with the target nucleus, denoted by N_h was also recorded for each event. For the low sensitive stacks N_T, defined by $g \geq 2g_{min}$ ($E_p \leq 280$ MeV), was used as an alternative measure of the target breakup.

Events occuring in the emulsion chambers were collected by "area scanning" the normally-incident beam in the 350 μm-thick target plates. Because of the limited volume of emulsion in which an event must be detected, there is an inherent bias against the detection of events that exhibit mainly low target-fragment multiplicities, although low shower particle and/or projectile fragment production contributes to this loss; such events are nominally a prerequisite for the presence of peripherally-produced PFs. To minimize this bias, the emulsion chambers were scanned under 22X oil objectives with 10X oculars, a combination which allows one to detect events with shower multiplicties $n_s \geq 10$ and $N_h \geq 1$ with high efficiency. Because PFs cannot be resolved within the target plate, particles emitted within the forward, fragmentation cone (0.20 mrad for PFs with $Z \geq 2$) in each event were examined at distances up to 4 cm from their origin, sufficient to attain complete resolution of the PFs, if present. Also, because of their high rates of ionization, PFs having $Z \geq 2$ were unambiguously resolved from Z=1 shower particles by inspection.

The identification of Z=2 PFs is unique when the multiplicities of the PFs are 3 and 4. For multiplicities of 2, a visual comparison of the track diameters enabled the observer to determine the (non) equality of the charges of the PFs. PFs of equal charges were deemed to be due to He nuclei, because the production of 2 PFs each with Z=3 or 4 is extremely rare. The smaller of two unequal charges was taken to be due to He. Only for single PF emission was absolute charge, estimation necessary. Although visual estimation of track diameters, i.e., charge was made in each case, our sample of 1He events can reasonably be expected to include some misidentified Z=3, and possibly Z=4, PFs. Estimates of the upper limits of the correction factors can be, and have been, applied to the 1He data to eliminate the effects of background Z=3,4 PFs.

Emulsion chambers and stacks are complemetary in this experiment. Specifically, the data collected from stacks are largely unbiased. In particular the identification of projectile-like helium and PFs is very accurate. Also, the background of low energy hydrogen tracks simulating a PF at the collision point is completely negligible within the fragmentation cone. However, the accuracy in determining the vector direction of particle tracks is degraded by distortion in the emulsion and the need to apply shrinkage-factor corrections to the vertical component of the track vectors. The advantages gained by use of chambers are that angular data are accurate, limited only by the accuracies of the microscope stage coordinates and the geometrical configuration of the chambers. Measurements are simplified and secondary reactions are reduced to a minimun because of the low average density of the chamber itself.

PROJECTILE AND TARGET-FRAGMENT DISTRIBUTIONS:

Table I presents the relative rates of production of projectile fragments form ^{16}O-Em interactions in nuclear emulsion at relativistic energies. The data used are minimum-bias events. No attempt was made to eliminate electromagnetically induced events. This was done to facilitate a comparison with results obtained from LS emulsions. The fraction of electromagnetic dissociation events is expected to be about 1% at 2.1A GeV and to be of order 10% at 200A GeV [6]. For the LS stacks, collisions with one PF and N_h = 0 are normally not observed in the scanning. Table I has been corrected for these losses as well as for a part of those with N_h = 1 (33%) N_h =2(10%), N_h=3(3%) and N_h = 4(1%). The former correction is directly taken from the HS data Judek [5] and the fraction of lost N_h = 1,2,3,4 collisions are obtained by comparing $\langle N_h \rangle$from Ref. 5 with $\langle N_T \rangle$ for collisions with one PF. The data are categorized according to Z_{max}, the maximum charge of the PFs emitted in each event, and, in the case of He, their multiplicities. We observe that PFs with $Z \geq 3$ are often accompanied by He PFs, i.e., by 1He in ~ 20%, and by 2He in ~ 2%, of the events of this class. Events grouped under "none" comprise those that involve the emission of Z=1 (shower) particles only, hence can be associated with complete disintegration of the projectile. The errors quoted in Table I for the HS stacks are taken from a binomial distribution and for the LS stacks a systematic error is included in the correction factor to compensate for the loss of small N_h events.

As we shall do henceforth, Table I compares the production of PFs from ^{16}O interactions in emulsion at E/A = 200 GeV with those observed at 2.1 (Ref. 5), 14.6 and 60 GeV. Due to possible systematic errors in the correction factors for the LS stacks, the HS and LS samples should preferably be compared separately. Both sets of observations clearly exhibit energy independence, the data agreeing to the extent that errors associated with the data points overlap in most channels. None-the-less, small systematic variations in specific reaction channels cannot be ruled out. As a particular example the 1He/3He ratio appears to increase between 2A GeV and 200A GeV, a variation whose significance lies at about the two standard deviation level at this stage. In Fig. 1 we show the data from HS emulsions for 2.1, 14.6, 60 and 200 GeV/nucleon. Again, the overall energy independence of the production channels is evident. In another experiment, Ref. 6, that used Fuji ET7B HS emulsion, the following percentages were obtained for ^{16}O- 200A GeV collisions: 16.8 ± 1.5, 12.0 ± 1.3, 5.9± 1.0, 0, 36.2 ± 2.0 and 29.1 ± 1.9; they compare favorably with our combined HS+LS data in Table I.

In Fig. 2a we interrelate the total charge of PFs ($Z \geq 2$), $\sum Z_{PF}$, produced in ^{16}O-Em interaction with the associated mean number $\langle N_h \rangle$ of heavily ionizing tracks emitted mainly from the target nucleus. The range of $\sum Z_{PF}$ varies from 0, i.e., when no PF ($Z \geq 2$) is emitted, to 8, when the total incident charge of the ^{16}O appears in the PFs. These data reveal that the degree of target excitation, as represented by $\langle N_h \rangle$, is strongly correlated with the sum of the charges carried by the PFs. Qualitatively, the greater the fragmentation of the projectile, i.e., the smaller the sum $\sum Z_{PF}$, the greater is the degree of fragmentation of the target. In Fig. 2b we examine $\langle N_h \rangle$ as a function of the number of singly charged particles falling inside the fragmentation cone (defined by $\theta < \theta_c$, where $\theta_c = 0.2/p_{inc}$) for events with no observed PFs. Again a strong dependence is seen which is qualitatively understandable as reflecting an anti-correlation between the target participants (as measured via $\langle N_h \rangle$) and the projectile spectators (as measured by the number of singly charged particles falling inside the fragmentation cone).

In Fig. 3 we show the similar behaviour for $\langle N_T \rangle$ where N_T, as stated before, contains all tracks with $dE/dx \geq 2\ (dE/dx)_{min}$ which means that tracks equivalent to protons with $E_p < 280$ MeV are included in the data. At 200A GeV, $\langle N_T \rangle$ is 3 units lower then $\langle N_h \rangle$ in the HS Stacks and we note that the difference between the observed quantities $\langle N_h \rangle$ and $\langle N_T \rangle$ is higher the fewer PF He nuclei that are emitted. The qualitative behaviour of the $\langle N_h \rangle$ and $\langle N_T \rangle$ correlations with the number of charges possessed by PFs is certainly the same. Specific points of interest are: i) the data exhibit, qualitatively, energy independence. ii) Target excitation depends only on $\sum Z_{PF}$, irrespective of the distribution of charges that contribute to the particular sum, and iii) $\langle N_h \rangle$ decreases approximately linearly with $\sum Z_{PF}$. We note that linearity may fail at low values of $\sum Z_{PF}$ when $\langle N_h \rangle$ exceeds 8, the demarcation point between the major light ($Z \leq 8$) and heavy ($Z \geq 35$) target groups in emulsion, indicative of a change in the effective mass of the target nucleus.

PROJECTILE FRAGMENTATION, Z=2:

The intrinsic spatial resolution attainable with emulsion chambers/stacks enables us to measure the projected angles θ_x and θ_y, and pseudorapidity η of the He fragments associated with the 200A GeV ^{16}O projectile. The angles θ_x and θ_y are the projections of the polar angle of emission of the PFs on the xy and yz planes, where z is the vector direction of the incident ion. Because θ_x and θ_y obey the same physics, they are presented as a single distribution in Fig. 4. The data are based on a total of 97 interactions, giving rise to 178 He PFs with multiplicities $1 \leq N_{He} < 3$. No 4He events were observed in this sample. The angular distribution is gaussian-shaped, with dispersion $\sigma(\theta_{xy}) = (20.5 \pm 1.0) \times 10^{-5}$ rad under the restriction that $|\theta_{xy}| \leq 50 \times 10^{-5}$ rad. Given that the incident momentum is 200A GeV/c, the corresponding (x or y) momentum component is estimated to be $\sigma(p_{xy}) = 155 \pm 8$ MeV/c, taking the average atomic mass number of the He PFs to be 3.78. Assuming isotropy in the projectile frame, $\sigma(p_{xy})$ is equivalent to the longitudinal momentum $\sigma(p_z)$, which permits favorable comparisons of this result with $\sigma(p_z) = 137 \pm 2$ MeV/c observed in early experiments on the fragmentation of 2.1A GeV ^{16}O nuclei.[2,8]

Fig. 5 presents the derived momentum dispersions $\sigma(p_{xy})$ of the He PFs as a function of the multiplicity of He PFs. The closed circles identify the 200A GeV ^{16}O data. These data are to be directly compared with the 2.1A GeV ^{16}O results plotted as open circles (HS stacks) and open triangles (LS stacks) [7]. Also shown in Fig. 5 by open squares are (unpublished) data on the momentum dispersions of 3He and 4He PFs from 2.1A GeV ^{12}C-CH_2 interactions obtained with the HISS facility [9]. For purposes of comparison, the dispersions are those obtained by fitting all momentum spectra to Gaussian distributions for $|p_{xy}| \leq 375$ MeV/c.

The only correction applied to the data shown in Fig. 5 was to the value of $\sigma(p_{xy})$ for the ^{16}O-1He datum of 200A GeV. As commented on above, these data were obtained from emulsion chambers, where the visual inspection of the diameters of the single vertical tracks of PFs was insufficient to resolve Z=2 from Z=3 (and possibly 4). Under the assumptions that i) our 1He data contain a background of events that include all 1Li PFs (unaccompanied by He), ii) given that the relative production rates of the 1He and 1Li channels are 13.5 and 3.3%, respectively, [5], and iii) that the momentum dispersion for a PF of mass A_F produced from a beam projectile A_B is $\sigma \propto [X(1-X)]^{1/2}$ where $X=A_F/A_B$, [3], we find that our 1He result should be increased by about 7% to correct for the presence of Li. Similarly, if, as an upper limit, we assume that all 1Be PFs are also included in our sample, then the estimated correction factor increases to about 11%. We have, therefore, applied a +9%(±2%) correction to our measured value of the momentum dispersion for the 200A GeV 1He, a correction equal to about one standard deviation of the experimental uncertainty.

We wish to point out that the 1He, as well as the 2He channel is the composite of all events having 1 (or 2) He PFs, irrespective of the presence of PFs $\geq$ 3. Upon separating the 1He events into those accompanied a) by Z=1 shower particles only and b) by PFs $Z \geq 3$, we find that the momentum dispersions of the He PFs are highly dependent on the topologies a) and b). As shown in Fig. 5 for the ^{16}O 1He data at 2.1A GeV (open circles with dashed error bars), the value of $\sigma(p_{xy})$ for 1He accompanied by Z=1 particles (only) is 22% <u>greater</u> than the composite average of 194 MeV/c, whereas $\sigma(p_{xy})$ for

1He with PFs $Z\geq 3$ is 20% <u>less</u> than the composite average. Hence, it is evident that the observed momentum (angular) distribution of 1He events in a given experiment depends markedly on the relative efficiencies for detecting these classes of 1He events.

Conclusions apparent from Fig. 5 are: i) The dispersions $\sigma(p_{xy})$ of He PFs from ^{16}O at 200A and 2.1A GeV are in good agreement, indicative of energy independence. ii) This energy independence, i.e., limiting fragmentation, also appears to extend to the individual He-multiplicity channnels as well, with the dispersions of the He decreasing with increasing He multiplicity, or alternatively, (see Fig. 2a) with decreasing target multiplicity $<N_h>$. iii)These general features are also observed in ^{12}C-CH_2 interactions, where the momentum distributions of the 3He and 4He PFs were attained with the HISS facility using magnetic rigidity and particle identification techniques. We stress, however, that there is a non-Gaussian contribution of PF-like He nuclei which is most significant for 1He events and gradually decreases with increasing number of He nuclei. It seems as if gentle processes of the type 3He, 4He or He+PF($Z\geq 3$) give momentum transfers well accounted for by thermal motion only, whereas for the 1He and possibly 2He channels collisions of a more violent kind become significant. The hatched area shows the region of the expected (constant) width from the liberation of He-nuclei at a fixed temperature[3].

At this stage of our investigations, correlations between shower particles and PFs have not been studied. Indeed, the number of shower particles, n_s, produced in events studied here rarely exceeds 50, with an average number in the range of ~ 20 to 25. Such events are characteristic of small nuclear involvement of the projectile.

The presentation of the emission angles of the He PFs in terms of pseudorapidiy η, as shown in Fig. 6, clearly identifies the particles at the highest value of η, e.g. $\eta > 8$, that are observed in the pseudorapidity distributions for low multiplicity ($n_s < 50$) ^{16}O-Em events at 200A GeV as beam-velocity fragments of the incident projectile [1].

The solid curve in Fig. 6 is the predicted η-distribution based on the ^{16}O- He spectrum measured at 2.1A GeV ($\sigma(p_z)$ = 137 MeV/c [2]). The observed value $<\eta> = 9.15 \pm 0.06$, with η in the range $7.6 \leq \eta \leq 13$, is in good agreement with the spectrum derived from the transformation of 2.1A GeV data to 200A GeV.

SUMMARY:

The angular and derived momentum distributions of the He PFs we have observed in ^{16}O-Em interactions at 200A GeV are characteristically Gaussian - shaped with widths σ that are comparable to those due to Fermi motion in the projectile nucleus. Of particular importance is the result that the "Fermi motion" and the σ of the momentum distribution of He PFs are, in fact, dependent on the multiplicity of the emitted He PFs, decreasing with increasing multiplicity, and, at a given multiplicity, dependent on the presence (or not) of PFs $Z \geq 3$ in final state. This behavior is, within the errors of our measurement, independent of beam energy, and at 2.1A GeV, is also exhibited in the He PF spectra from ^{12}C-CH_2 interactions.

As a practical result, this observation extends the validity of the assumption of energy independence of the parameter σ used in the estimation of the primary energies of fragmenting nuclei, e.g., in cosmic rays, from the angular distributions of HE PFs - provided the dependence of the momentum distributions on He PF multiplicities is taken into account.

The general feature of projectile fragmentation in ^{16}O-Em interactions, derived from an intercomparison of the results at E/A= 2.1, 14.6, 60 and 200 GeV is that energy independence, i.e. limiting fragmentation, is sustained in the interval $2 \leq E/A \leq 200$ GeV. In addition to the angular dependence of He PFs with the He multiplicity cited above, this energy independence encompasses i) the production rates of PFs, $Z \geq 2$, and ii) the charge and multiplicity distributions and their dependence on target multiplicities, N_h or N_T. The possible indications of energy dependences in selected reaction channels make desirable the accumulation of higher statistics. We find that the associated target-fragment multiplicities decrease monotonically with increasing total charge $\sum Z_{PF}$ of the emitted PFs ($Z \geq 2$). Thus, we deduce that the degrees of excitation energy of the projectile and target nuclei are directly correlated, an effect that is furthermore independent of beam energy.

ACKNOWLEDGEMENT:

Kudos to the CERN staff of the PS and SPS for their outstanding performance in producing the ^{16}O beam for this experiment, with special credit to G. Vanderhaege, K. Ratz, N. Doble, P. Grafstrom, M. Reinharz, H. Sletten and J. Wotschack. We are grateful for the assistance of A. Oskarsson in monitoring the beam during the exposures of the emulsion, and, most importantly, for the contributions given by the scanning/measuring staffs within the collaboration, The financial support from the Swedish NFR. The German Federal Minister of Research and Technology, The National Natural Science Foundation of China, and the U.S. Department of Energy under Contract DE-AC03-76SF00098 and NSF in the USA are gratefully acknowledged.

REFERENCES:

[1] EMU-01 collaboration, M.I. Adamovich, et al., Phys, Lett. B201, 397 (1988).

[2] D.E. Greiner, P.J. Lindstrom, H.H. Heckman, B. Cork and F.S. Bieser, Phys. Rev. Lett. 35, 152 (1975).

[3] A.S. Goldhaber, Phys. Lett. B53, 306 (1974).

[4] S. Garpman, I. Otterlund, S. Persson and K. Soderstrom, Nucl. Instr. and Methods in Phys. Res. A269, 134 (1988).

[5] B.Judek, 14th Int. Cosmic Ray Conf. Munich, Germany Vol. 7, 2342 (1975). Also private communication (1988)

[6] N. Ardito, et al., Europhys. Lett. 6, 131(1988)
D. Olson, private communication (1988).

[7] B.Jakobsson, R.Kullberg and I.Otterland, Lett al Nuovo Cimento 15, 444 (1976)

[8] H.H. Heckman, D.E. Greiner, P.J. Lindstrom, and H. Shwe, Phys. Rev. C17, 1735 (1988).

[9] P.J. Lindstrom, private communication (1988).

FIGURE CAPTIONS:

Fig. 1 The fraction (%) of minimum bias events having $Z \geq 3$ (inclusive), none (no $Z \geq 2$), 1He, 2He, 3He and 4He (exclusive) in ^{16}O-Em interactions at E/A= 2.1, 14.6, 60 and 200 GeV incident energy for HS stacks. Errors shown are statistical only. The dashed lines give the mean values assuming energy independence.

Fig. 2 a) Mean number of heavily ionizing target fragments ($g \geq 1.4 g_{min}$), N_h, plotted versus $\sum Z_{PF}$, the total charge of PFs ($Z \geq 2$) emitted in ^{16}O-Em collisions The fragmentation channels are indicated. The open squares, closed squares, open circles and closed circles are the symbols for the E/A= 2.1, 14.6, 60 and 200 GeV data, respectively. b) The inset shows $\langle N_h \rangle$ as a function of the number of singly charged particles inside the fragmentation cone $n_{Z=1}(\theta < \theta_c)$ for events having no PFs with $Z \geq 2$. Values of θ_c are 1.0, 3.3 and 13 mrad for E/A = 200, 60 and 14.6 GeV, respectively. Symbols are the same as defined for a).

Fig.3 A plot similar to Fig. 2 showing $\langle N_T \rangle$ versus $\sum Z_{PF}$ where T-fragments have $dE/dx \geq 2(dE/dx)_{min}$ in E/A= 2.1, 14.6, 60 and 200 GeV reactions.

Fig. 4 Projected polar angles θ_x and θ_y of the projectile fragments for ^{16}O-Em interactions at 200A GeV. The solid curve is the Gaussian fit to the data, $|\theta_{xy}| \leq 50 \times 10^{-5}$ rad. The width of the the distribution is $\sigma(\theta_{xy}) = (20.5 \pm 1.0) \times 10^{-5}$ rad, corresponding to a momentum $\sigma(p_{xy}) = 155 \pm 8$ MeV/c. The insert figures defines the angles θ_x and θ_y

Fig. 5 Momentum widths $\sigma(p_{xy})$ versus multiplicity of the He PFs from ^{16}O-Em interactions at 200A GeV (closed circles) at 2.1A GeV in HS emulsions (open circles) and LS emulsions (open triangles), and from ^{12}C-CH_2 interactions at 2.1A GeV (open squares). Note the shift in the upper (^{12}C) abscissa. The 2.1A GeV-^{16}O data for 1He shown with dashed error bars give the momentum widths for the 1He PF events with Z=1 particles only (upper value) and for 1He PF events with PFs $3 \leq Z \leq 6$ (lower value). The hatched region is the one to be expected from independent emission of He from a thermal system.

Fig. 6 Pseudorapidity distribution of He PFs. The smooth curve is the expected distribution extrapolated from 2.1A GeV.

TABLE I Relative production rates, in percent, of projectile fragments from 2.1, 14.6, 60 and 200 GeV/nucleon ^{16}O nuclei in nuclear emulsion. Data are categorized by the maximum charge (and its multiplicity) of the emitted PFs. Indicated in the last column are detector type and sensitivity, i.e. high(HS) and low (LS)

Energy E/A GeV	Events	1He	2He	3He	4He	Z>2	None	Detector
2.1	1192	13.5±1.0	10.2±0.9	6.7±0.7	0.7±0.2	36.6±1.4	32.4±1.4	Ilford G5 HS
	269	14.1±2.3	9.4±1.9	9.0±1.8	0.3±0.2	37.2±3.0	30.0±3.0	Ilford K2 LS
Total	1461	13.6±0.9	10.1±0.8	7.1±0.7	0.6±0.1	36.7±1.3	32.0±1.2	Both
14.6	417	19.7±2.0	14.4±1.7	7.2±1.3	0.2±0.2	30.9±2.3	27.6±2.2	NIKFI BR-2 HS
	106	18.7±4.0	9.4±3.0	5.1±2.3	0.0	37.1±5.3	29.7±5.0	Ilford K5 LS
Total	523	19.3±1.7	13.4±1.5	6.7±1.1	0.2±0.2	32.1±2.0	27.9±2.0	Both
60	402	15.2±1.8	8.7±1.4	7.2±1.3	1.0±0.5	38.1±2.4	29.9±2.3	NIKFI BR-2 HS
	1001	17.7±1.6	11.5±1.2	5.8±0.9	0.3±0.2	31.7±2.5	33.1±2.1	Ilford K5 LS
Total	1403	17.0±1.5	10.7±0.9	6.2±0.7	0.5±0.1	33.5±2.0	32.2±1.6	Both
200	1196	16.1±1.1	10.6±0.9	5.8±0.7	0.4±0.2	37.3±1.4	29.8±1.3	NIKFI BR-2 HS
	732	18.4±1.8	14.6±1.6	5.1±1.0	0.2±0.2	33.9±2.9	27.8±2.2	Ilford K5 LS
Total	1928	17.0±1.0	12.1±0.8	5.6±0.7	0.3±0.2	36.0±1.3	29.0±1.2	Both

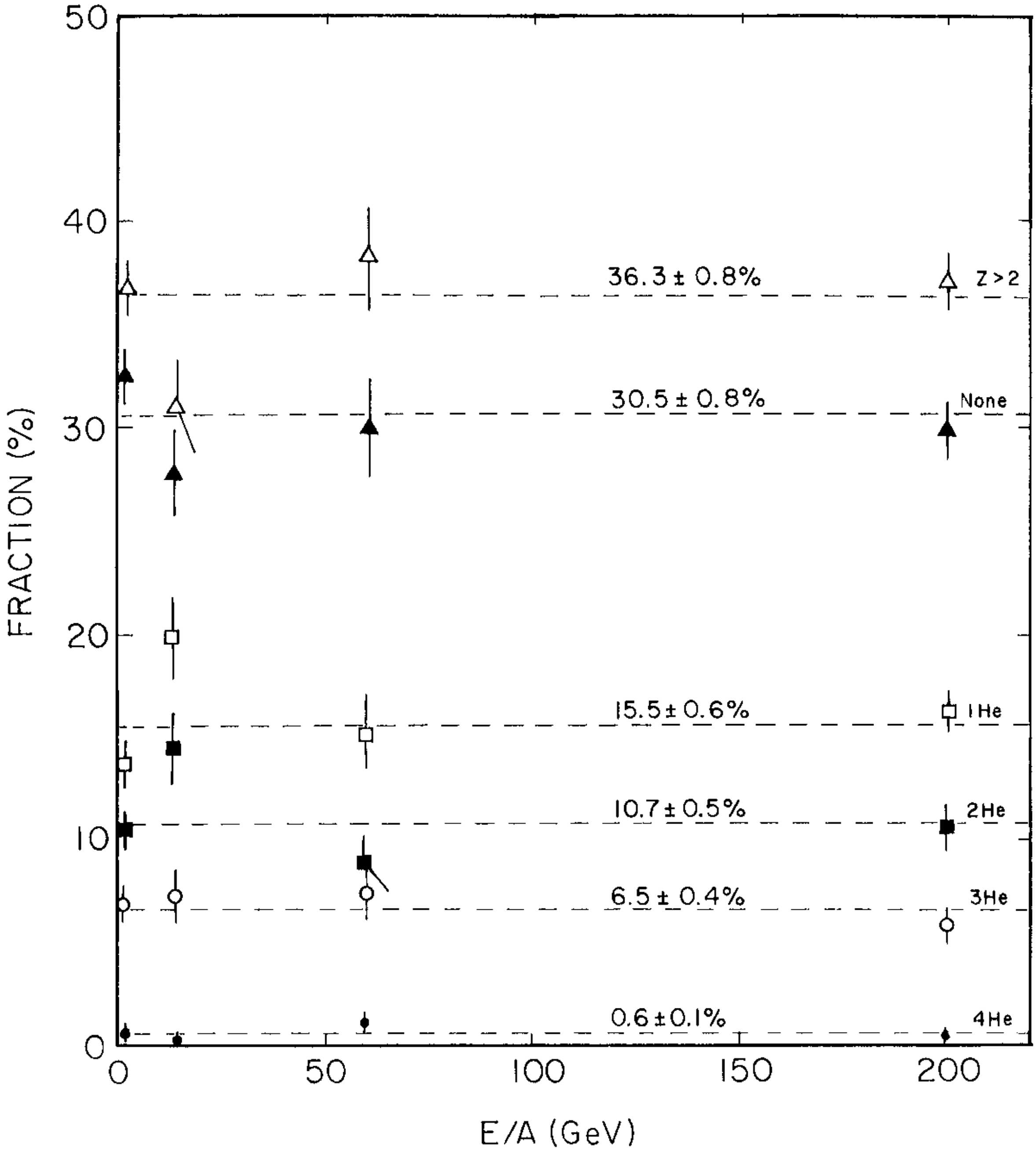

XBL 891-343

Fig. 1

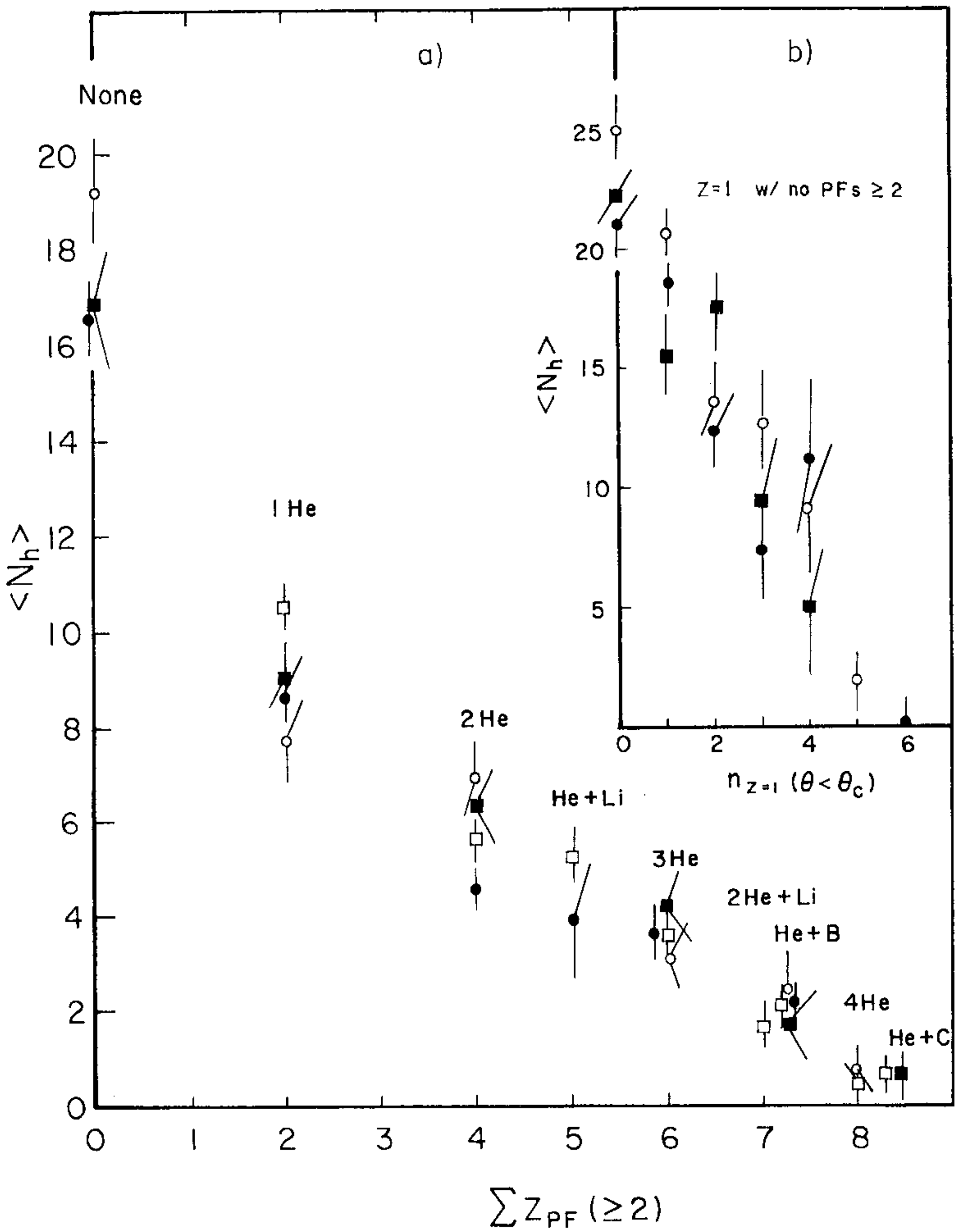

XBL 891-344

Fig. 2

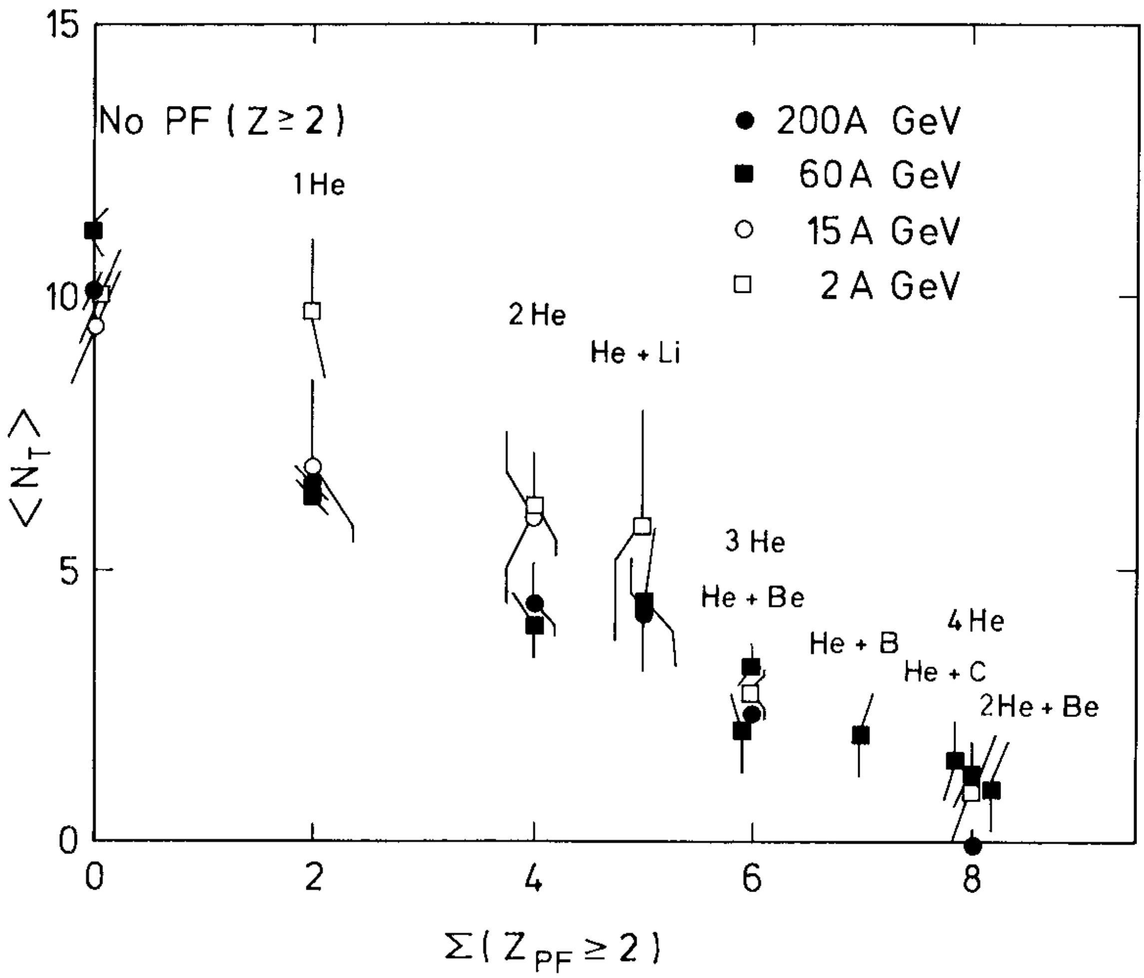

XBL 891-345

Fig. 3

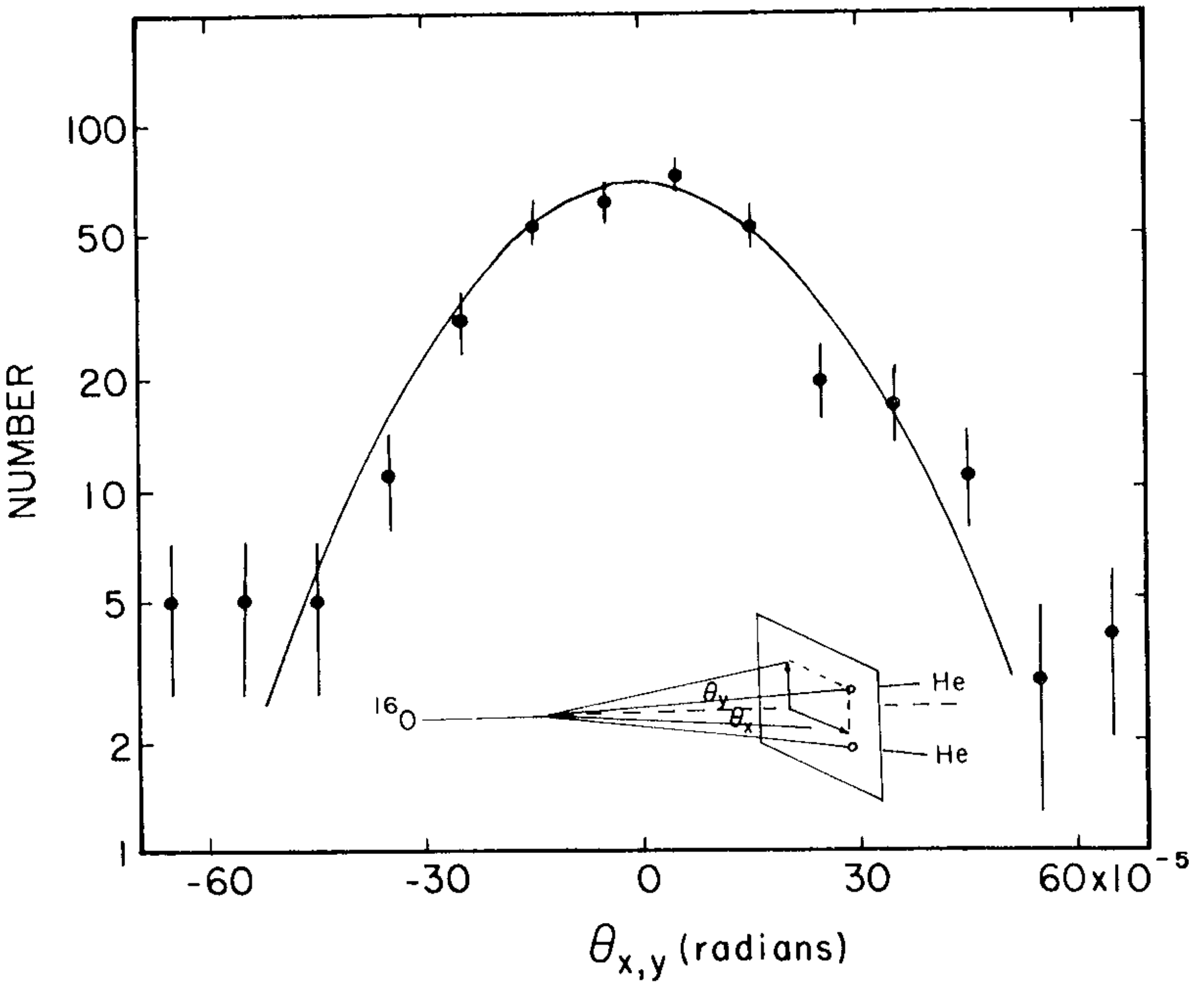

XBL 886-2063

Fig. 4

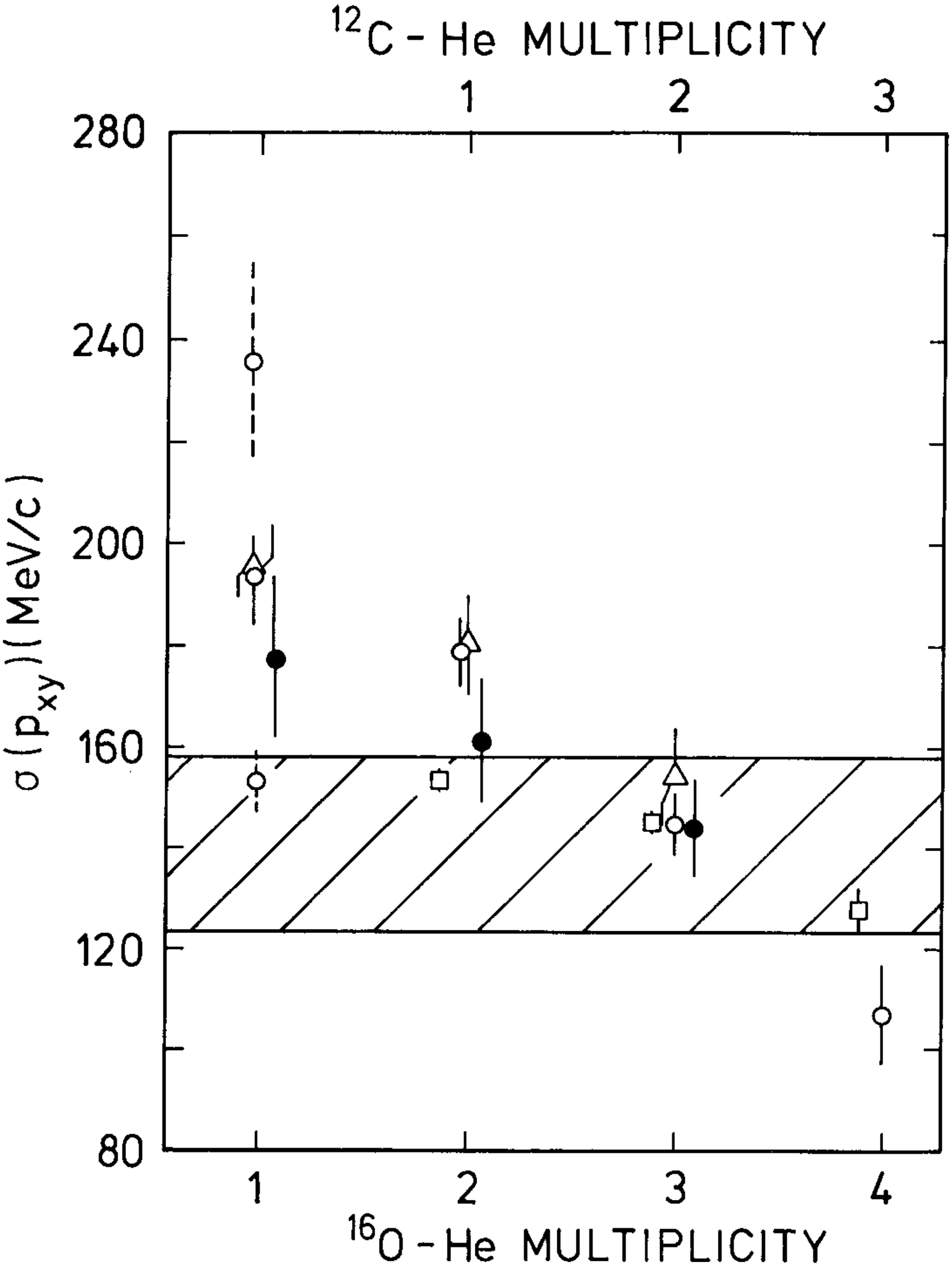

XBL 891-342

Fig. 5

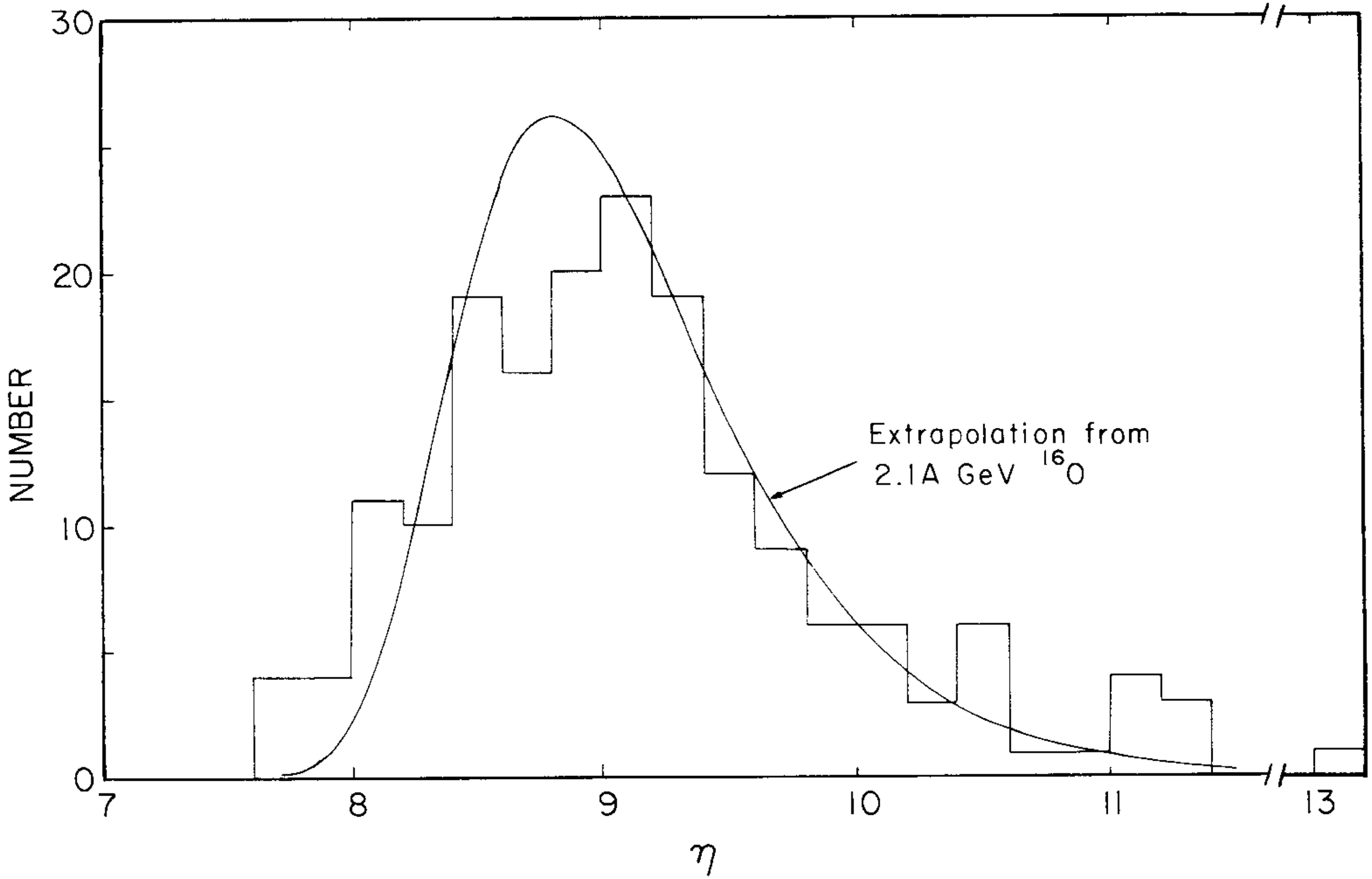

XBL 886-2066

Fig. 6